

$(g - 2)_{e,\mu}$ in an extended inverse type-III seesaw

Pablo Escribano^a, Jorge Terol-Calvo^{b,c}, Avelino Vicente^{a,d}

^(a) Instituto de Física Corpuscular, CSIC-Universitat de València, 46980 Paterna, Spain

^(b) Instituto de Astrofísica de Canarias, C/ Vía Láctea, s/n, 38205 La Laguna, Tenerife, Spain

^(c) Universidad de La Laguna, Departamento de Astrofísica, La Laguna, Tenerife, Spain

^(d) Departament de Física Teòrica, Universitat de València, 46100 Burjassot, Spain

pablo.escribano@ific.uv.es, jorgetc@iac.es, avelino.vicente@ific.uv.es

Abstract

There has been a long-standing discrepancy between the experimental measurements of the electron and muon anomalous magnetic moments and their predicted values in the Standard Model. This is particularly relevant in the case of the muon $g - 2$, which has attracted a remarkable interest in the community after the long-awaited announcement of the first results by the Muon $g - 2$ collaboration at Fermilab, which confirms a previous measurement by the E821 experiment at Brookhaven and enlarges the statistical significance of the discrepancy, now at 4.2σ . In this paper we consider an extension of the inverse type-III seesaw with a pair of vector-like leptons that induces masses for neutrinos at the electroweak scale and show that one can accommodate the electron and muon anomalous magnetic moments, while being compatible with all relevant experimental constraints.

1 Introduction

The charged leptons anomalous magnetic moments,

$$a_\ell = \frac{g_\ell - 2}{2}, \quad (1)$$

with $\ell = e, \mu, \tau$, are known to be powerful probes of New Physics (NP) effects, potentially hidden in virtual loop contributions. Interestingly, there has been a long-standing discrepancy between the Standard Model (SM) prediction for the electron and muon anomalous

magnetic moments and their experimentally determined values [1–7]. In the case of the electron $g - 2$, the significance is slightly below $\sim 3\sigma$, and hence not very significant at the moment. In contrast, the deviation has become particularly relevant in the case of the muon $g - 2$, in particular after the Muon $g - 2$ experiment at Fermilab has published its long-awaited first results [8]. Their measurement of a_μ perfectly agrees with the result obtained by the E821 experiment at Brookhaven [5] and, consequently, disagrees with the SM. Their combination leads to a 4.2σ discrepancy with the SM prediction compiled by the theory community in [9]. In summary, the current status of the electron and muon $g - 2$ can be quantified as ¹

$$\begin{aligned}\Delta a_e &= a_e^{\text{exp}} - a_e^{\text{SM}} = (-87 \pm 36) \times 10^{-14}, \\ \Delta a_\mu &= a_\mu^{\text{exp}} - a_\mu^{\text{SM}} = (25.1 \pm 5.9) \times 10^{-10}.\end{aligned}\tag{2}$$

New measurements and more refined theoretical calculations are definitely required to assess the relevance of these anomalies, and confirm whether these intriguing deviations are hints of NP [12], SM contributions not correctly taken into account or just statistical fluctuations. ² However, it is tempting to interpret them as a signal of the presence of new states beyond the SM (BSM). In this case, the $g - 2$ anomalies may hide valuable information about the shape of the underlying model. In particular, the sign difference between Δa_e and Δa_μ and the sizable value of $|\Delta a_e|$ would indicate that the NP contributions do not scale with the square of the charged lepton masses [15]. This calls for a non-trivial extension of the SM.

The inverse type-III seesaw model (ISS3) is obtained by replacing the fermionic $SU(2)_L$ singlets in the original inverse type-I seesaw [16] by $SU(2)_L$ triplets. This variant has already been studied [17–23], although not extensively, and many of its phenomenological features are still to be investigated. ³ In fact, there are several phenomenological directions of interest in the ISS3. The fact that triplets couple to the SM gauge bosons allow for new production mechanisms at the LHC, where one can also look for lepton number violating signatures. Lepton flavor violation might also be an interesting subject to explore in this model, which may offer some differences with respect to the more common inverse type-I seesaw [30]. Finally, the potentially sizable mixing between the charged components of the type-III triplet and the SM charged leptons may also lead to observable $Z \rightarrow \ell_i^+ \ell_j^-$ decays with $i \neq j$. We refer to [31] for a recent analysis of these and other relevant observables in the presence of light fermion triplets.

¹The status of the electron $g - 2$ has recently changed by a new measurement of the fine-structure constant [10]. The new value differs by more than 5σ to the previous one and affects the electron $g - 2$ anomaly, which gets reduced to just 1.6σ and flips sign, see [11]. We will not include these results in our analysis, but note that it would be straightforward to accommodate a positive Δa_e in our model, as shown in Sec. 4.

²The theoretical calculation of the electron and muon anomalous magnetic moments is a challenging task and has led to some controversies along the years. For instance, a recent calculation of the hadronic vacuum polarization contribution by the Budapest-Marseilles-Wuppertal collaboration [13] brings the SM prediction for the muon $g - 2$ into agreement with the experimental value, hence ruling out any discrepancy. However, it has been pointed out that this result in turn leads to some tension with electroweak data [14].

³See also [24, 25] for discussions of generalized inverse seesaw models, including versions with Dirac neutrinos, [26–28] for three references studying the phenomenology of light fermion triplets and [29] for a recent work on the inverse seesaw with spontaneous violation of lepton number.

While many models have been put forward to address the discrepancy between theory and experiment in the electron and muon $g - 2$, the main motivation for the ISS3 is not to accommodate the existing deviations, but to induce non-zero masses for neutrinos. It is therefore natural to investigate whether the model can account for the experimental values for the electron and muon anomalous magnetic moments in the region of parameter space that can reproduce the observed neutrino masses and leptonic mixing angles, measured in oscillation experiments, while being compatible with the bounds obtained at colliders and low-energy experiments. In this paper we show that these constraints preclude the ISS3 from inducing large contributions to $(g - 2)_{e,\mu}$, making it impossible to address the existing discrepancies. This motivates a minimal extension of the model that keeps its most relevant features but provides additional ingredients to generate sizable contributions to the electron and muon $g - 2$. We find that the introduction of a pair of vector-like (VL) lepton doublets with sizable couplings to electrons and muons can explain the anomalies and simultaneously satisfy all the experimental constraints. It is the aim of this paper to study the electron and muon $g - 2$ in this model, which we denote as the ISS3VL.

The muon $g - 2$ has been considered in a wide variety of contexts, in many cases in connection to neutrino mass generation. This includes models based on the inverse seesaw mechanism [32–40] and/or with VL leptons [41–59]. See also [60] for a recent work in the context of a radiative neutrino mass model including triplet fermions. Finally, we note that the muon $g - 2$ has also been considered as a motivation for a muon collider [61–63].

The rest of the manuscript is organized as follows. In Sec. 2 the basic features of the ISS3VL model are introduced, including the generation of charged and neutral lepton masses. In Sec. 3 we compute the charged lepton $g - 2$ values and provide simplified approximate expressions. A numerical analysis is performed in Sec. 4. After arguing that the pure ISS3 model cannot address the anomalies, we explore the parameter space of the ISS3VL model and obtain results for the electron and muon $g - 2$ compatible with the relevant experimental constraints. Finally, we discuss our results and conclude in Sec. 5. Appendices A and B contain additional details, such as analytical expressions for the couplings of interest to our calculation and full expressions for the charged lepton anomalous magnetic moments.

2 The model

The ISS3VL is an extension of the leptonic sector of the SM with the addition of six right-handed Weyl fermion $SU(2)_L$ triplets with vanishing hypercharge, Σ_A and Σ'_A ($A = 1, 2, 3$), and a VL copy of the SM lepton doublet, L_L and L_R . The Σ_A and Σ'_A triplets are introduced in order to generate neutrino masses via the inverse type-III seesaw mechanism.⁴ They can be distinguished by their different lepton numbers, with $L(\Sigma) = +1$ and $L(\Sigma') = -1$. Nevertheless, lepton number will be explicitly broken in the ISS3VL. Therefore, this lepton number assignment is arbitrary. The new fermionic fields L_L and L_R have the same representations under the $SU(3)_c \times SU(2)_L \times U(1)_Y$ gauge group, and both are doublets under $SU(2)_L$. The full particle content of the ISS3VL model and the representations of all fields under the $SU(3)_c \times SU(2)_L \times U(1)_Y$ gauge group are shown in Tab. 1.

⁴In order to simplify the notation, we will not denote the chirality of the $\Sigma_A \equiv \Sigma_{RA}$ and $\Sigma'_A \equiv \Sigma'_{RA}$ fermions explicitly.

	q_L	u_R	d_R	ℓ_L	e_R	Σ	Σ'	L_L	L_R	H
$SU(3)_C$	3	$\bar{\mathbf{3}}$	$\bar{\mathbf{3}}$	1	1	1	1	1	1	1
$SU(2)_L$	2	1	1	2	1	3	3	2	2	2
$U(1)_Y$	$\frac{1}{6}$	$\frac{2}{3}$	$-\frac{1}{3}$	$-\frac{1}{2}$	-1	0	0	$-\frac{1}{2}$	$-\frac{1}{2}$	$\frac{1}{2}$
GENERATIONS	3	3	3	3	3	3	3	1	1	1

Table 1: Particle content of the ISS3VL. q_L , ℓ_L , u_R , d_R , e_R and H are the usual SM fields.

As usual, the SM $SU(2)_L$ doublets can be decomposed as

$$q_L = \begin{pmatrix} u \\ d \end{pmatrix}_L, \quad \ell_L = \begin{pmatrix} \nu \\ e \end{pmatrix}_L, \quad H = \begin{pmatrix} H^+ \\ H^0 \end{pmatrix}. \quad (3)$$

The Σ and Σ' triplets can also be decomposed into $SU(2)_L$ components. With $\Sigma_A = (\Sigma^1, \Sigma^2, \Sigma^3)_A$, they can be conveniently written in the usual 2×2 matrix notation according to (the same holds for the primed states)

$$\Sigma_A = \frac{1}{\sqrt{2}} \vec{\tau} \cdot \vec{\Sigma}_A = \begin{pmatrix} \Sigma_A^0/\sqrt{2} & \Sigma_A^+ \\ \Sigma_A^- & -\Sigma_A^0/\sqrt{2} \end{pmatrix}, \quad (4)$$

where τ_A are the usual Pauli matrices and the states with well-defined electric charge are given by

$$\Sigma_A^0 = \Sigma_A^3, \quad \Sigma_A^\pm = \frac{\Sigma_A^1 \mp i \Sigma_A^2}{\sqrt{2}}. \quad (5)$$

Finally, the VL leptons $L_{L,R}$ can be decomposed as

$$L_{L,R} = \begin{pmatrix} N \\ E \end{pmatrix}_{L,R}. \quad (6)$$

Under the above working assumptions, the most general Yukawa Lagrangian allowed by all symmetries can be written as

$$\mathcal{L}_Y = \mathcal{L}_Y^{\text{SM}} + \mathcal{L}_Y^{\text{ISS3}} + \mathcal{L}_Y^{\text{VL}}, \quad (7)$$

where

$$-\mathcal{L}_Y^{\text{SM}} = \bar{q}_L Y_u u_R \tilde{H} + \bar{q}_L Y_d d_R H + \bar{\ell}_L Y_e e_R H + \text{h.c.} \quad (8)$$

is the usual SM Lagrangian, with $\tilde{H} = i \tau_2 H^*$, and $Y_{u,d,e}$ are 3×3 Yukawa matrices in flavor space. Here and in the following we omit $SU(2)_L$ contractions and flavor indices to simplify the notation. The terms

$$-\mathcal{L}_Y^{\text{ISS3}} = \sqrt{2} \bar{\Sigma} Y_\Sigma \ell_L \tilde{H}^\dagger + \bar{\Sigma} M_\Sigma \Sigma'^c + \frac{1}{2} \bar{\Sigma}' \mu \Sigma'^c + \text{h.c.}, \quad (9)$$

correspond to the usual ISS3 extension. Here Y_Σ , M_Σ and μ are 3×3 matrices, the latter two with dimensions of mass. Finally, the VL leptons allows for additional Lagrangian terms, given by

$$-\mathcal{L}_Y^{\text{VL}} = \sqrt{2}\bar{\Sigma}\lambda_L L_L \tilde{H}^\dagger + \bar{e}_R \lambda_R L_L \tilde{H}^\dagger + \bar{L}_L M_L L_R + \bar{\ell}_L \epsilon L_R + \text{h.c.} . \quad (10)$$

Here λ_L and λ_R are dimensionless 3×1 vectors and M_L a parameter with dimensions of mass. The 1×3 vector ϵ has dimensions of mass, and will be assumed to vanish for simplicity.⁵ The guiding principle when writing the Yukawa Lagrangian in Eq. (7), in particular the piece in Eq. (9), is the conservation of lepton number, only allowed to be broken by the $\bar{\Sigma}' \mu \Sigma'^c$ term. In fact, in the absence of the Majorana mass μ , the Lagrangian would have an additional $U(1)_L$ global symmetry. In the following we will consider $\mu \ll M_\Sigma$, corresponding to a *slightly broken lepton number*, in the spirit of the original inverse seesaw mechanism.

The scalar potential of the model is the same as in the SM,

$$\mathcal{V} = m^2 |H|^2 + \lambda |H|^4 , \quad (11)$$

with m^2 a parameter with dimensions of $[\text{mass}]^2$. Therefore, electroweak symmetry breaking takes place in the usual way, with

$$\langle H \rangle = \frac{1}{\sqrt{2}} \begin{pmatrix} 0 \\ v \end{pmatrix} , \quad (12)$$

with $v \simeq 246$ GeV the SM Higgs vacuum expectation value. After electroweak symmetry breaking, several terms in the Yukawa Lagrangian in Eq. (7) induce mixings in the neutral and charged lepton sectors. In the bases $n \equiv n_L = (\nu_L, (\Sigma^0)^c, (\Sigma'^0)^c, N_L, N_R^c)$, $f_L = (e_L, (\Sigma^+)^c, (\Sigma'^+)^c, E_L)$ and $f_R = (e_R, \Sigma^-, \Sigma'^-, E_R)$, the neutral and charged fermion mass terms read

$$-\mathcal{L}_m = \frac{1}{2} \bar{n}^c \mathcal{M}_N n + \bar{f}_L \mathcal{M}_C f_R + \text{h.c.} , \quad (13)$$

with the mass matrices given by

$$\mathcal{M}_N = \begin{pmatrix} 0 & m_D^T & 0 & 0 & 0 \\ m_D & 0 & M_\Sigma & m_L & 0 \\ 0 & M_\Sigma^T & \mu & 0 & 0 \\ 0 & m_L^T & 0 & 0 & M_L \\ 0 & 0 & 0 & M_L & 0 \end{pmatrix} , \quad (14)$$

and

$$\mathcal{M}_C = \begin{pmatrix} m_e & \sqrt{2} m_D^T & 0 & 0 \\ 0 & 0 & M_\Sigma & 0 \\ 0 & M_\Sigma^T & \mu & 0 \\ m_R^T & \sqrt{2} m_L^T & 0 & -M_L \end{pmatrix} . \quad (15)$$

Here we have defined

$$m_D = \frac{v}{\sqrt{2}} Y_\Sigma , \quad m_e = \frac{v}{\sqrt{2}} Y_e , \quad m_L = \frac{v}{\sqrt{2}} \lambda_L \quad \text{and} \quad m_R = \frac{v}{\sqrt{2}} \lambda_R . \quad (16)$$

⁵The ϵ term contributes to the electron, muon and tau masses and is therefore constrained to be small.

We note that the neutral lepton mass matrix \mathcal{M}_N is 11×11 , whereas the charged lepton mass matrix \mathcal{M}_C is 10×10 . They can be brought to diagonal form by means of the unitary transformations \mathcal{U} , \mathcal{V}^L and \mathcal{V}^R , defined by

$$\mathcal{U}^* \mathcal{M}_N \mathcal{U}^\dagger = \text{diag} (m_{N_i}) , \quad (17)$$

$$\mathcal{V}^{L*} \mathcal{M}_C \mathcal{V}^{R\dagger} = \text{diag} (m_{\chi_i}) , \quad (18)$$

resulting in the 11 neutral (Majorana) fermion masses m_{N_i} and the 10 charged (Dirac) fermion masses m_{χ_j} , with $i = 1, \dots, 11$ and $j = 1, \dots, 10$. In the following we will assume the hierarchy of energy scales

$$\mu \ll m_D, m_L, m_R \ll M_\Sigma, M_L , \quad (19)$$

which allows one to obtain approximate expressions for the physical lepton masses. We note that a small μ parameter is justified through 't Hooft naturalness criterion [64]. In the case of the neutral leptons, one finds 3 light states, to be identified with the standard light neutrinos. Their mass matrix is approximately given by

$$m_\nu \approx m_D^T (M_\Sigma^T)^{-1} \mu M_\Sigma^{-1} m_D , \quad (20)$$

with corrections of the order of the small ratios $(m_D/M_\Sigma)^2$ and $(m_L/M_L)^2$. This result is proportional to the μ parameter. It is then clear that sizable Y_Σ Yukawa couplings and triplets at the TeV scale are consistent with light neutrino masses due to the suppression by the μ term. This is the inverse seesaw mechanism.

3 Charged lepton anomalous magnetic moments

The charged lepton magnetic moments can be described by the effective Hamiltonian [65]

$$\mathcal{H} = c_{ij} \bar{\ell}_j \sigma_{\mu\nu} P_R \ell_i F^{\mu\nu} + \text{h.c.} , \quad (21)$$

where $P_R = (1 + \gamma_5)/2$ is the usual right-handed chiral projector, $F^{\mu\nu}$ the electromagnetic field strength tensor and ℓ_i denote the light charged lepton mass eigenstates, equivalent in our scenario to $\chi_{1,2,3}$. The anomalous magnetic moment is given in terms of the real components of the diagonal c coefficients as

$$a_i = -\frac{2m_i}{e} (c_{ii} + c_{ii}^*) = -\frac{4m_i}{e} \text{Re} c_{ii} , \quad (22)$$

whereas the imaginary components would in turn induce electric dipole moments.

The ISS3VL has the ingredients to induce large charged lepton anomalous magnetic moments, namely, light new particles with sizable couplings to the charged leptons. In the ISS3VL, new contributions to the charged lepton anomalous magnetic moments are induced at the 1-loop level, as shown in Fig. 1. While these diagrams also exist in the SM, in the ISS3VL the mass eigenstates N_i and χ_i include new heavy states beyond the SM leptons.

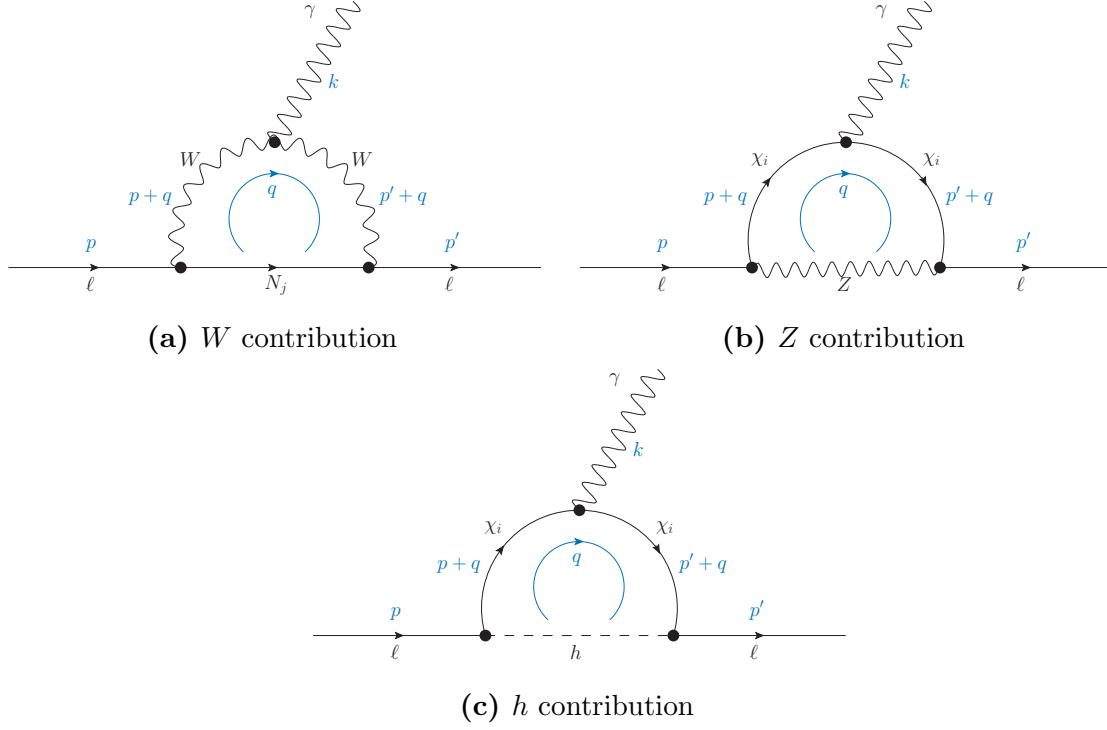


Figure 1: Feynman diagrams that contribute to the charged lepton anomalous magnetic moment at the 1-loop level in the ISS3VL. Here χ_i and N_j denote any of the charged and neutral lepton mass eigenstates, respectively. Momenta are shown in blue.

Moreover, the couplings of the SM states get modified due to mixings with the new BSM

states. The amplitudes of these Feynman diagrams are given by

$$\begin{aligned}
i \mathcal{M}_\ell^W &= \int \frac{d^4 q}{(2\pi)^4} \bar{u}_\ell(p') \gamma^\beta \left[(g_{\chi N W}^L)_{\ell j} P_L + (g_{\chi N W}^R)_{\ell j} P_R \right] i \frac{\not{q} + m_{N_j}}{q^2 - m_{N_j}^2} \\
&\quad \gamma^\alpha \left[(g_{\chi N W}^L)_{j\ell} P_L + (g_{\chi N W}^R)_{j\ell} P_R \right] \frac{-i \left(g_{\alpha\bar{\alpha}} - \frac{(p+q)_\alpha (p+q)_{\bar{\alpha}}}{m_W^2} \right)}{(p+q)^2 - m_W^2} \Gamma^{\mu\bar{\alpha}\bar{\beta}} \\
&\quad \frac{-i \left(g_{\beta\bar{\beta}} - \frac{(p'+q)_\beta (p'+q)_{\bar{\beta}}}{m_W^2} \right)}{(p'+q)^2 - m_W^2} u_\ell(p) \varepsilon_\mu^*, \tag{23}
\end{aligned}$$

$$\begin{aligned}
i \mathcal{M}_\ell^Z &= \int \frac{d^4 q}{(2\pi)^4} \bar{u}_\ell(p') \gamma^\beta \left[(g_{\chi Z}^L)_{i\ell} P_L + (g_{\chi Z}^R)_{i\ell} P_R \right] i \frac{(\not{p}' + \not{q}) + m_{\chi_i}}{(p'+q)^2 - m_{\chi_i}^2} \\
&\quad \gamma^\mu \left[(g_{\chi\gamma}^L)_{ii} P_L + (g_{\chi\gamma}^R)_{ii} P_R \right] i \frac{(\not{p} + \not{q}) + m_{\chi_i}}{(p+q)^2 - m_{\chi_i}^2} \gamma^\alpha \left[(g_{\chi Z}^L)_{\ell i} P_L + (g_{\chi Z}^R)_{2i} P_R \right] \\
&\quad \frac{-i \left(g_{\alpha\beta} - \frac{q_\alpha q_\beta}{m_Z^2} \right)}{q^2 - m_Z^2} u_\ell(p) \varepsilon_\mu^*, \tag{24}
\end{aligned}$$

$$\begin{aligned}
i \mathcal{M}_\ell^h &= \int \frac{d^4 q}{(2\pi)^4} \bar{u}_\ell(p') \left[(g_{\chi h}^L)_{i\ell} P_L + (g_{\chi h}^R)_{i\ell} P_R \right] i \frac{(\not{p}' + \not{q}) + m_{\chi_i}}{(p'+q)^2 - m_{\chi_i}^2} \\
&\quad \gamma^\mu (-ie) i \frac{(\not{p} + \not{q}) + m_{\chi_i}}{(p+q)^2 - m_{\chi_i}^2} \left[(g_{\chi h}^L)_{\ell i} P_L + (g_{\chi h}^R)_{\ell i} P_R \right] \frac{i}{q^2 - m_h^2} u_\ell(p) \varepsilon_\mu^*. \tag{25}
\end{aligned}$$

Here $P_L = (1 - \gamma_5)/2$ is the left-handed chiral projector, ε_μ is the photon polarization 4-vector and the couplings $g_{\chi N W}^{L,R}$, $g_{\chi Z}^{L,R}$, $g_{\chi\gamma}^{L,R}$, $g_{\chi h}^{L,R}$ and Γ are defined in Appendix A. A sum over the indices i, j is implicit in these expressions, while ℓ is the index of the external charged lepton. We have computed the amplitudes in Eqs. (23)-(25) with the help of `Package-X` [66]. After projecting onto the operator in Eq. (21), one obtains analytical expressions for the contributions to the c coefficient, which can then be translated into contributions to the charged leptons $g - 2$ thanks to the relation in Eq. (22). The total ISS3VL contribution to Δa_ℓ can be written as ⁶

$$\Delta a_\ell = \Delta a_\ell(W) + \Delta a_\ell(Z) + \Delta a_\ell(h). \tag{26}$$

Assuming that the ISS3VL states N_i and χ_i are much heavier than the SM states (this is, assuming the mass hierarchy $m_{N_i}, m_{\chi_i} \gg m_h, m_W, m_Z \gg m_\ell$), one can find approximate

⁶Higher-order contributions, such as those induced by 2-loop Barr-Zee diagrams [67], will be neglected in the following.

expressions for the three contributions:

$$\Delta a_\ell(W) \simeq \frac{m_\ell}{32\pi^2 m_W^2} \left\{ \frac{4}{3} m_\ell \left[1 - \frac{3m_W^2}{4m_{N_i}^2} \left(11 + 6 \log \frac{m_W^2}{m_{N_i}^2} \right) \right] (C_{\chi NW}^2)_{i\ell} \right. \\ \left. + m_{N_i} \left[1 - \frac{3m_W^2}{m_{N_i}^2} \left(3 + 2 \log \frac{m_W^2}{m_{N_i}^2} \right) \right] (D_{\chi NW}^2)_{i\ell} \right\}, \quad (27)$$

$$\Delta a_\ell(Z) \simeq \frac{m_\ell}{32\pi^2 m_Z^2} \left\{ -\frac{5}{3} m_\ell (C_{\chi Z}^2)_{i\ell} + m_{\chi_i} (D_{\chi Z}^2)_{i\ell} \right\}, \quad (28)$$

$$\Delta a_\ell(h) \simeq \frac{m_\ell}{32\pi^2 m_{\chi_i}^2} \left\{ \frac{1}{3} m_\ell (C_{\chi h}^2)_{i\ell} + m_{\chi_i} (D_{\chi h}^2)_{i\ell} \right\}. \quad (29)$$

Here we have defined the coupling combinations

$$(C_Y^2)_{i\ell} \equiv |(g_Y^L)_{i\ell}|^2 + |(g_Y^R)_{i\ell}|^2 \quad \text{and} \quad (D_Y^2)_{i\ell} \equiv (g_Y^L)_{i\ell} (g_Y^R)_{i\ell}^* + (g_Y^L)_{i\ell}^* (g_Y^R)_{i\ell}, \quad (30)$$

with $Y = \chi NW, \chi Z, \chi h$. Again, the indices i and ℓ denote the BSM particle running in the loop and the charged lepton, respectively. We have checked that Eqs. (27), (28) and (29) reproduce the ISS3VL contributions to the charged leptons anomalous magnetic moments in very good approximation. Nevertheless, full expressions are given in Appendix B and used in the numerical analysis presented in the next Section. We note that $\Delta a_\ell(W)$, $\Delta a_\ell(Z)$ and $\Delta a_\ell(h)$ contain contributions proportional to $m_N g_{\chi NW}^L g_{\chi NW}^R$, $m_\chi g_{\chi Z}^L g_{\chi Z}^R$ and $m_\chi g_{\chi h}^L g_{\chi h}^R$, respectively, proportional to the mass of the fermion in the loop. These terms are usually called *chirally-enhanced contributions* and they typically dominate due to the large masses of the heavy fermions running in the loop.

4 Phenomenological discussion

We proceed now to present our phenomenological exploration of the parameter space of the ISS3VL.

4.1 Experimental constraints

Let us first discuss how we fix the parameters of the model in order to reproduce the measured lepton masses and mixings. The Y_e Yukawa matrix will be fixed to the same values as in the SM, hence neglecting corrections from the mixing between the SM charged lepton states and the charged components of the Σ and Σ' triplets. These corrections are multiplicative and enter at order $\sim (m_D/M_\Sigma)^2$ and can thus be safely neglected. The same argument applies to the mixing with the charged components of the VL leptons, which enter at order $\sim (m_R/M_L)^2$. Without loss of generality, we will work in the basis in which M_Σ is diagonal and μ is a general complex symmetric matrix. In this case, Y_Σ and μ must be properly fixed in order to reproduce neutrino oscillation data [68]. In principle, one can fix the entries of μ to some input values and express the Y_Σ Yukawa matrix by means of the master parametrization [69, 70], which in this case reduces to a modified Casas-Ibarra

parametrization [71]. While this is perfectly valid, one generically obtains Y_Σ matrices with sizable off-diagonal entries unless some input parameters are tuned very finely. Due to the strong constraints from the non-observation of lepton flavor violating processes, this excludes most of the parameter points. Therefore, we take the alternative choice of fixing Y_Σ to specific input values, diagonal for simplicity, and computing μ by inverting Eq. (20) as

$$\mu = M_\Sigma^T (m_D^T)^{-1} m_\nu m_D^{-1} M_\Sigma, \quad (31)$$

where $m_\nu = U_\nu^* \widehat{m}_\nu U_\nu^\dagger$. Here U_ν is the leptonic mixing matrix measured in oscillation experiments, given in terms of 3 mixing angles and 3 CP-violating phases. Eq. (31) guarantees that all the parameter points considered in our numerical analysis are compatible with neutrino oscillation data. In our analysis we use the results of the global fit in [68] and we consider both normal and inverted neutrino mass orderings.

In order to ensure compatibility with constraints from flavor and electroweak precision data we use the bounds derived in [31], where a global analysis is performed in the context of general type-III seesaw models. The limits provided in this reference are given for the 3×3 matrix η , defined in our case in terms of the matrices

$$M_D = \begin{pmatrix} m_D & \\ & 0 \end{pmatrix} \quad \text{and} \quad M = \begin{pmatrix} 0 & M_\Sigma \\ M_\Sigma^T & \mu \end{pmatrix}, \quad (32)$$

as

$$\begin{aligned} \eta &= \frac{1}{2} M_D^\dagger (M^\dagger)^{-1} M^{-1} M_D \\ &= \frac{1}{2} m_D^\dagger (M_\Sigma^*)^{-1} \left[\mathbb{I}_3 + \mu^* (M_\Sigma^\dagger)^{-1} (M_\Sigma^T)^{-1} \mu \right] M_\Sigma^{-1} m_D \\ &\approx \frac{1}{2} m_D^\dagger (M_\Sigma^*)^{-1} M_\Sigma^{-1} m_D. \end{aligned} \quad (33)$$

In our analysis, we make sure that the bounds are respected by computing the η matrix in all the parameter points considered. As we will explain below, these limits preclude the ISS3 model from being able to address the electron and muon $g - 2$ anomalies. Furthermore, we also consider the decay widths for the processes $Z \rightarrow \ell^+ \ell^-$ and $h \rightarrow \ell^+ \ell^-$, with $\ell = e, \mu$, which are also affected due to the mixing of the light charged leptons with the heavy states in our model. They are computed as

$$\Gamma(Z \rightarrow \ell^+ \ell^-) = \frac{m_Z^3}{12\pi v^2} \left[\left| (g_{\chi Z}^V)_{\ell\ell} \right|^2 + \left| (g_{\chi Z}^V)_{\ell\ell} \right|^2 \right], \quad (34)$$

$$\Gamma(h \rightarrow \ell^+ \ell^-) = \frac{m_h}{8\pi} \left[\left| (g_{\chi h}^L)_{\ell\ell} \right|^2 + \left| (g_{\chi h}^R)_{\ell\ell} \right|^2 \right], \quad (35)$$

with $g_{\chi Z}^V = g_{\chi Z}^L + g_{\chi Z}^R$ and $g_{\chi Z}^A = g_{\chi Z}^R - g_{\chi Z}^L$. The $Z \rightarrow \ell^+ \ell^-$ decay turns out to provide an important constraint in our setup. In fact, it has been recently pointed out that this process potentially correlates with the charged leptons $g - 2$ [72]. We define the ratios

$$R_{Z\ell\ell} = \frac{\Gamma(Z \rightarrow \ell^+ \ell^-)}{\Gamma_{\text{SM}}(Z \rightarrow \ell^+ \ell^-)}, \quad (36)$$

with $\Gamma_{\text{SM}}(Z \rightarrow \ell^+\ell^-)$ the SM predicted decay width, and impose that $R_{Z\ell\ell}$ lies within the 95% CL range, which we estimate to be $0.995 < R_{Zee} < 1.003$ and $0.993 < R_{Z\mu\mu} < 1.006$ [73]. Regarding the Higgs boson decays, no constraints are actually obtained from them, since at present there is no hint for $h \rightarrow e^+e^-$ and evidence for $h \rightarrow \mu^+\mu^-$ was only obtained recently [74]. Therefore, they will be considered as predicted observables, potentially correlated with Δa_ℓ [72, 75].

Finally, we also impose bounds from collider searches. The type-III seesaw triplets have been searched for at the LHC in multilepton final states, both by ATLAS [76] and CMS [77, 78]. No excess above the expected SM backgrounds has been found, hence allowing the experimental collaborations to set limits on the triplet mass and couplings. Using a data sample obtained with proton collisions at $\sqrt{s} = 13$ TeV and an integrated luminosity of 35.9 fb^{-1} , CMS reports a lower bound on the triplet mass of 840 GeV at 95% confidence level, if the triplet couplings are assumed to be lepton flavor universal [78]. While the flavor structure of the triplet couplings to leptons does not affect the heavy triplet pair production cross-sections, driven by gauge interactions, it has an impact on the flavor composition of the multilepton signature. The limit changes if the assumption of lepton flavor universal couplings is dropped, resulting in a more stringent bound when the triplet couples mainly to electrons and a more relaxed bound when the triplet couples mainly to taus, with values ranging between 390 and 930 GeV. The bounds from the CMS collaboration in [78] are applied in our analysis. However, since the CMS analysis focuses on the standard type-III seesaw scenario, and does not consider the particular features of the ISS3VL model, several simplifying assumptions must be made. We define

$$B_{A\alpha} = \frac{\Gamma(\Sigma_A^0 \rightarrow \ell_\alpha + \text{boson}) + \Gamma(\Sigma_A^+ \rightarrow \ell_\alpha + \text{boson})}{\sum_\alpha [\Gamma(\Sigma_A^0 \rightarrow \ell_\alpha + \text{boson}) + \Gamma(\Sigma_A^+ \rightarrow \ell_\alpha + \text{boson})]}, \quad (37)$$

where Σ_A^0 and Σ_A^+ are the quasi-Dirac pairs approximately formed by the mass eigenstates $N_i + N_j$ and $\chi_i + \chi_j$, respectively. An implicit sum over the bosons in the final states is also assumed, including decays to W^\pm , Z and h . For instance, in a parameter point in which the lightest BSM states are mainly composed by the components of the Σ_1 triplet, we have $i = 4$, $j = 5$ and $\Gamma(\Sigma_1^0 \rightarrow \ell_\alpha + \text{boson}) \equiv \Gamma(N_4 \rightarrow W^\pm \ell^\mp) + \Gamma(N_4 \rightarrow Z\nu_\alpha) + \Gamma(N_4 \rightarrow h\nu_\alpha) + \Gamma(N_5 \rightarrow W^\pm \ell^\mp) + \Gamma(N_5 \rightarrow Z\nu_\alpha) + \Gamma(N_5 \rightarrow h\nu_\alpha)$. We note that $B_{Ae} + B_{A\mu} + B_{A\tau} = 1$. This is the quantity that we use to confront each quasi-Dirac pair with the limits given on Figure 3 of [78]. Our approach approximates the total heavy triplet pair production to $pp \rightarrow \Sigma_A^0 \Sigma_A^+$, which is known to give the dominant contribution at the LHC [79]. Furthermore, we apply two additional simplifications. First, since CMS assumes the neutral and charged components of the triplet to be mass degenerate, we adopt a conservative approach and take the lowest of them as the triplet mass to be used in the analysis. And second, we do not apply the CMS bounds to quasi-Dirac triplet pairs that are largely mixed with the VL leptons, since their production cross-section is clearly reduced with respect to the pure triplet case.⁷ We believe that our assumptions conservatively adapt the CMS limits in [78] to our scenario. We note that ATLAS finds a similar bound on the triplet mass in the flavor

⁷In practice, we do not apply the CMS bounds in cases with large mixings. For instance, they are not applied to χ_i Dirac states that combine a left-handed fermion that is mostly a type-III triplet with a right-handed fermion that is mostly a VL lepton, or vice versa.

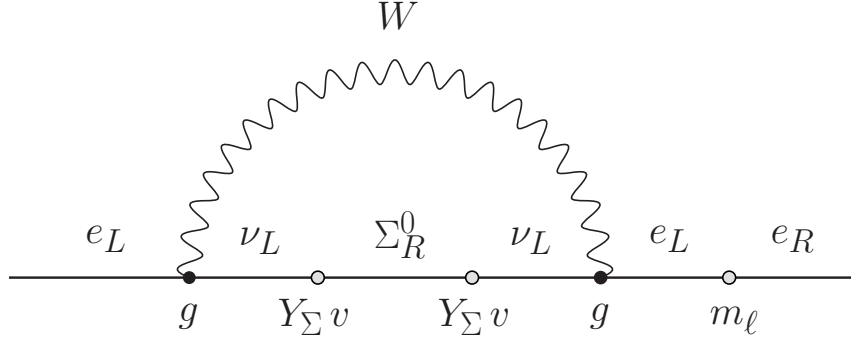


Figure 2: Dominant W contribution in the ISS3. Mass insertions are represented by white blobs.

universal scenario, ruling out (at 95% confidence level) values below 790 GeV [76]. Finally, LHC limits on VL leptons strongly depend on their decay modes, namely the flavor of the charged leptons produced in the final states [80]. In our analysis we will consider $M_L \geq 500$ GeV, a conservative value that guarantees compatibility with current LHC searches. These limits are expected to be improved by the end of the LHC Run-III [81].

4.2 $(g - 2)_{e,\mu}$ in the ISS3

Before studying the electron and muon $g - 2$ in the ISS3VL, let us discuss these observables in the context of the *pure* ISS3 and show that this model cannot induce large contributions, hence being unable to address the existing discrepancies. One can easily reach this conclusion by estimating the size of the dominant contributions to the charged lepton $g - 2$. Fig. 2 shows the dominant W contribution. Assuming that the chirally-enhanced term in Eq. (27) dominates, one finds the estimate

$$\Delta a_\ell(W) \sim \frac{1}{32\pi^2} \frac{m_N m_\ell}{m_W^2} g^2 \left(\frac{m_D}{M_\Sigma} \right)_{\ell\ell}^2 \frac{m_\ell}{v} \sim 10^{-3} \frac{m_N m_\ell^2}{m_W^3} \eta_{\ell\ell}. \quad (38)$$

We highlight the relevance of the m_ℓ/v factor in Eq. (38). This factor is not apparent when inspecting the analytical expressions for the couplings in Appendix A. In fact, the individual contributions to $\Delta a_\ell(W)$ by the neutral fermions in the loop are larger than their sum, $\Delta a_\ell(W)$, by a factor $\sim v/m_\ell$. Therefore, a strong cancellation among them takes place. This cancellation can be easily understood due to the chirality-flipping nature of the dipole moment operator in Eq. (21). The factor m_ℓ/v is required to flip the chirality of the fermion line and induce a contribution to a dipole moment. One can now consider $m_N = 1$ TeV to obtain

$$\Delta a_e(W) \sim 5 \cdot 10^{-13} \eta_{ee}, \quad (39)$$

$$\Delta a_\mu(W) \sim 2 \cdot 10^{-8} \eta_{\mu\mu}. \quad (40)$$

Since η_{ee} and $\eta_{\mu\mu}$ are constrained to be smaller than $\sim 10^{-4}$ [31], these contributions fail to address the electron and muon $g - 2$ anomalies by several orders to magnitude. The same

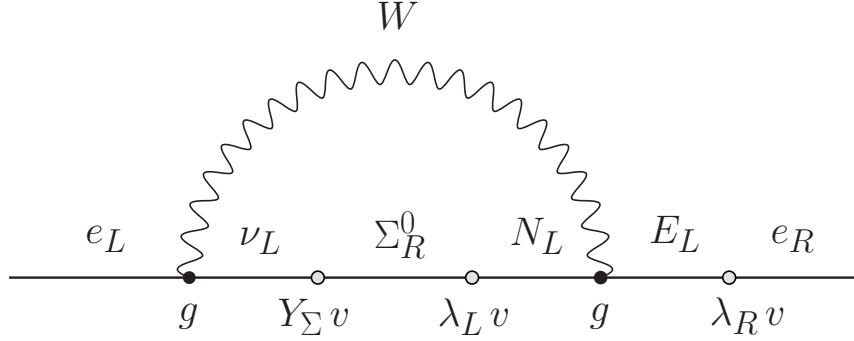


Figure 3: Dominant W contribution in the ISS3VL. Mass insertions are represented by white blobs.

argument can be applied to the Z and h contributions to find that they are actually even more suppressed. In summary, the suppression by the m_ℓ/m_W chirality flip and the stringent bounds on $\eta_{\ell\ell}$ imply that the ISS3 cannot induce sizable contributions to the electron and muon anomalous magnetic moments. We now proceed to show that the additional ingredients in our extended model can alter this conclusion.

4.3 $(g - 2)_{e,\mu}$ in the ISS3VL

As already discussed, the ISS3 cannot induce large contributions to the charged leptons anomalous magnetic moments. Therefore, we now consider its ISS3VL extension. In this case one has W contributions such as the one shown in Fig. 3. We can now derive an analogous estimate, along the same lines as in the case of the ISS3. One finds

$$\Delta a_\ell(W) \sim \frac{1}{32\pi^2} \frac{m_N m_\ell}{m_W^2} g^2 \left(\frac{m_D}{M_\Sigma} \right)_{\ell\ell} \frac{m_L}{M_L} \frac{m_R}{M_L} \sim 10^{-3} \frac{m_N m_\ell m_L m_R}{m_W^2 M_L^2} \sqrt{\eta_{\ell\ell}}. \quad (41)$$

One can now choose $m_N = 1$ TeV, $M_L = 500$ GeV, $m_L = 200$ GeV and $m_R = 10$ GeV to obtain

$$\Delta a_e(W) \sim 6 \cdot 10^{-10} \sqrt{\eta_{ee}}, \quad (42)$$

$$\Delta a_\mu(W) \sim 10^{-7} \sqrt{\eta_{\mu\mu}}. \quad (43)$$

Therefore, even after the suppression given by $\sqrt{\eta_{\ell\ell}} \lesssim 10^{-2}$ these W contributions can address the current discrepancies with the electron and muon $g - 2$ measurements. We note that the loop in Fig. 3 is proportional to the product $Y_\Sigma \lambda_L \lambda_R$ which, as shown below, will be crucial for the resulting values for Δa_ℓ in the ISS3VL model. Similar h contributions are also found, again proportional to the $Y_\Sigma \lambda_L \lambda_R$ product. Therefore, the model is in principle capable of producing sizable contributions to the electron and muon $g - 2$. We now proceed to confirm this by performing a detailed numerical analysis of the parameter space of the model. Since we are interested in Δa_e and Δa_μ , we fix $(\lambda_L)_3 = (\lambda_R)_3 = 0$ and randomly scan within the following parameter ranges:

Parameter	Min	Max
$(M_\Sigma)_{ii}$	850 GeV	1.5 TeV
M_L	500 GeV	1.5 TeV
$(Y_\Sigma)_{ii}$	0.05	0.2
$(\lambda_L)_1$	0.1	$\sqrt{4\pi}$
$(\lambda_L)_2$	$-\sqrt{4\pi}$	-0.1
$(\lambda_R)_1$	0.05	0.5
$(\lambda_R)_2$	0.05	0.5

Some comments about the chosen ranges are in order. First, the ranges for the mass parameters $(M_\Sigma)_{ii}$ and M_L have been selected following the discussion on LHC bounds of Sec. 4.1. Many of the parameter points in our scan were ruled out due to LHC searches for triplets, but we also find that a substantial fraction pass the test. The ranges for the Yukawa couplings have been chosen in order to maximize the resulting Δa_ℓ . The usual ISS3 Yukawas $(Y_\Sigma)_{ii}$ have been scanned around their maximal values compatible with the η_{ii} bounds. A relative sign between $(\lambda_L)_1$ and $(\lambda_L)_2$ has been introduced in order to obtain $\Delta a_e < 0$ and $\Delta a_\mu > 0$, as required by the experimental hints. Finally, the corrections to $\Gamma(Z \rightarrow \ell^+\ell^-)$ tend to be too large unless $(\lambda_R)_{1,2} \lesssim 0.5$.

Our results are based on a random scan with 50.000 parameter points, out of which about 12% – 13% pass all the experimental tests. We have selected normal neutrino mass ordering. However, we have also run a second scan with inverted ordering and found the same qualitative results. As already explained, we consider a scenario with diagonal Y_Σ and M_Σ matrices. In this case, the lepton mixing angles encoded in the matrix U_ν are generated by the off-diagonal entries of the μ matrix and all lepton flavor violating processes are strongly suppressed. For this reason, the bounds on the η_{ij} entries, with $i \neq j$, are easily satisfied. In contrast, the bounds on the diagonal elements of the η matrix turn out to be very important, removing a significant amount of the parameter points considered and implying the approximate bounds $(Y_\Sigma)_{11} \lesssim 0.2$ and $(Y_\Sigma)_{22} \lesssim 0.15$ for triplet masses of the order of the TeV. Another very important constraint in our setup is provided by the decay $Z \rightarrow \ell^+\ell^-$. The mixing between the SM charged leptons and the new charged BSM states from the Σ and Σ' triplets and $L_{L,R}$ VL doublets reduces $\Gamma(Z \rightarrow \ell^+\ell^-)$ with respect to its SM value. This has a strong impact on the m_D/M_Σ and m_R/M_L ratios. Since these ratios must be sizable in order to induce large contributions to Δa_ℓ , see Fig. 3, this limit is crucial for the correct evaluation of our scenario. Finally, the CMS limits discussed in Sec. 4.1 also have an impact, discarding some of the parameter points in our scan.

Our choice of a diagonal Y_Σ (in the basis in which M_Σ is diagonal too) implies that the mixing among different triplets is typically very small. In this case, and unless there is a large mixing with the VL neutral leptons, two of the heavy neutral mass eigenstates are given in good approximation by the $\Sigma_1 - \Sigma'_1$ quasi-Dirac pair and couple mainly to electrons. Similarly, two of the heavy neutral mass eigenstates are approximately given by the $\Sigma_2 - \Sigma'_2$ quasi-Dirac pair and couple mainly to muons. Therefore, the discussion in the previous Section implies that one expects a strong correlation between Δa_e and the product $(Y_\Sigma)_{11} (\lambda_L)_1 (\lambda_R)_1$, as well as between Δa_μ and the product $(Y_\Sigma)_{22} (\lambda_L)_2 (\lambda_R)_2$.

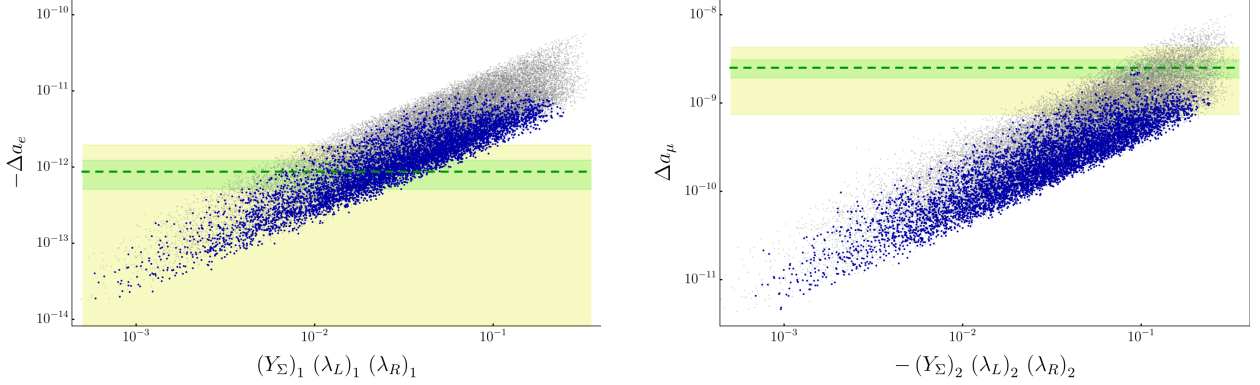


Figure 4: Δa_e (left) and Δa_μ (right) as a function of the product $(Y_\Sigma)_{ii} (\lambda_L)_i (\lambda_R)_i$. Blue dots correspond to parameter points that pass all the experimental constraints, whereas gray points are experimentally excluded. The horizontal dashed lines represent the central values for Δa_e and Δa_μ , whereas 1σ (3σ) regions are displayed as yellow (green) bands.

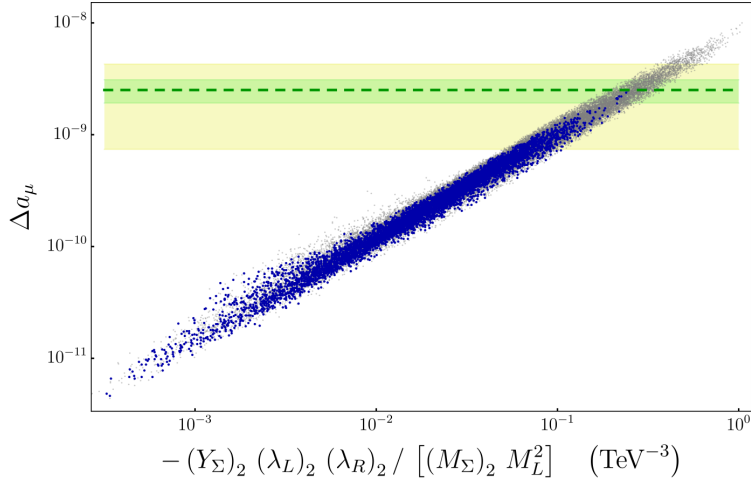


Figure 5: Δa_μ as a function of the combination $(Y_\Sigma)_{22} (\lambda_L)_2 (\lambda_R)_2 / [(M_\Sigma)_2 M_L^2]$. Dashed line, horizontal bands and color code as in Fig. 4.

This is clearly shown in Fig. 4. The left side of this figure shows Δa_e , whereas the right side displays results for Δa_μ , in both cases as a function of the said parameter combinations. Here, and in the following figures, parameter points that pass all the experimental constraints are displayed in blue color, whereas gray points are excluded for one or several of the reasons explained above, but included in the figure for illustration purposes. The horizontal dashed line represents the central value for Δa_ℓ , while 1σ (3σ) regions are displayed as yellow (green) bands. The first and most important result shown in this figure is that the ISS3VL can indeed explain the electron and muon $g - 2$ anomalies. In the case of the electron, one can easily find fully valid parameter points within the 1σ region, corresponding to values of $(Y_\Sigma)_{11} (\lambda_L)_1 (\lambda_R)_1$ in the ballpark of $\sim 0.01 - 0.05$. In fact, one can even exceed the experimental hint. In contrast, the muon $g - 2$ can only be explained within 1σ in a narrow region of the parameter space, with $(Y_\Sigma)_{22} (\lambda_L)_2 (\lambda_R)_2 \sim 0.1$. This is due to the combination of constraints that apply to our setup. Fig. 4 also confirms the

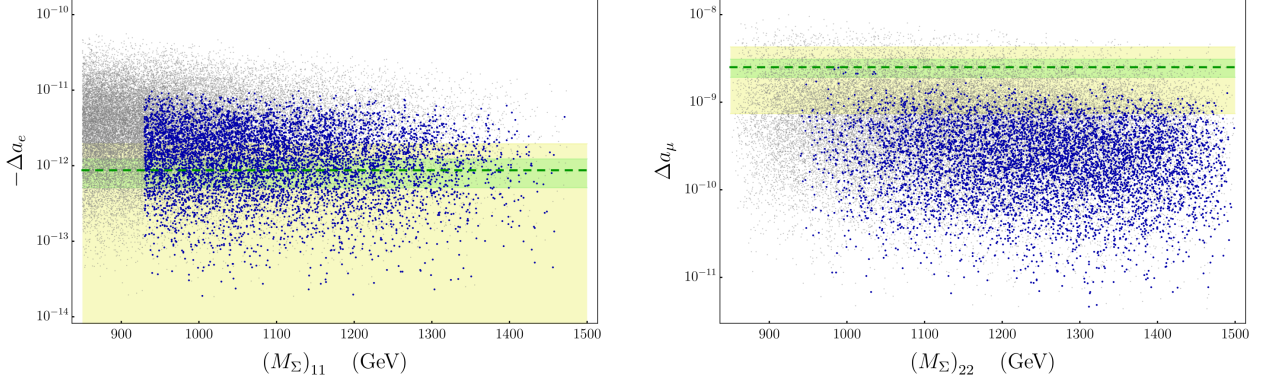


Figure 6: Δa_e (left) and Δa_μ (right) as a function of $(M_\Sigma)_{11}$ and $(M_\Sigma)_{22}$, respectively. Dashed line, horizontal bands and color code as in Fig. 4.

correlations with the product $(Y_\Sigma)_{ii} (\lambda_L)_i (\lambda_R)_i$, as we expected from the arguments given in the previous Section. The correlation is even more pronounced in terms of the combination $(Y_\Sigma)_{ii} (\lambda_L)_i (\lambda_R)_i / [(M_\Sigma)_i M_L^2]$, as shown in Fig. 5 for the case of the muon $g - 2$. This implies that the Feynman diagram in Fig. 3 indeed provides one of the dominant contributions to Δa_ℓ .

An example parameter point that achieves Δa_e and Δa_μ values in agreement with the central values in Eq. (2) is given by

$$(M_\Sigma)_{ii} = 1 \text{ TeV}, \quad M_L = 630 \text{ GeV}, \quad (44)$$

and

$$(Y_\Sigma)_{ii} = 0.117, \quad (\lambda_L)_1 = 0.6, \quad (\lambda_L)_2 = -\sqrt{4\pi}, \quad (\lambda_R)_1 = 0.1, \quad (\lambda_R)_2 = 0.25. \quad (45)$$

We note that a large $|(\lambda_L)_2|$, close to the non-perturbativity regime, is required to obtain a muon $g - 2$ in agreement with the central value. While in principle this is perfectly fine, one can relax this restriction with additional contributions to the muon $g - 2$. For instance, we expect this to happen in a non-minimal version of our model with more than just one generation of VL leptons or including singlet VL leptons.

Fig. 6 shows the dependence of Δa_ℓ on $(M_\Sigma)_{ii}$. On the left side, Δa_e is shown as a function of $(M_\Sigma)_{11}$, whereas the right side panel shows Δa_μ as a function of $(M_\Sigma)_{22}$. As explained above, these are the parameters that determine the masses of the triplets that couple mainly to electrons and muons, respectively. Therefore, as expected, the NP contributions decrease for larger values of $(M_\Sigma)_{ii}$. However, given the limited range over which these parameters were scanned, the reduction is not very strong. A lower bound $(M_\Sigma)_{11} \gtrsim 930 \text{ GeV}$ is clearly visible on the left-side panel. This is due to the fact that lower $(M_\Sigma)_{11}$ values would lead to lighter triplets, excluded by CMS searches. The dependence on M_L , the VL mass, is shown in Fig. 7 for the case of the muon $g - 2$. One can clearly see in this plot, as well as in the previous ones, that the density of valid parameter points gets reduced for low masses. This is because low $(M_\Sigma)_{ii}$ and/or M_L often lead to exclusion due to the $\Gamma(Z \rightarrow \ell^+ \ell^-)$ constraint.

We turn now our attention to the predictions of our setup. Fig. 8 shows the predicted values for the ratios

$$R_{h\ell\ell} = \frac{\Gamma(h \rightarrow \ell^+ \ell^-)}{\Gamma_{\text{SM}}(h \rightarrow \ell^+ \ell^-)}, \quad (46)$$

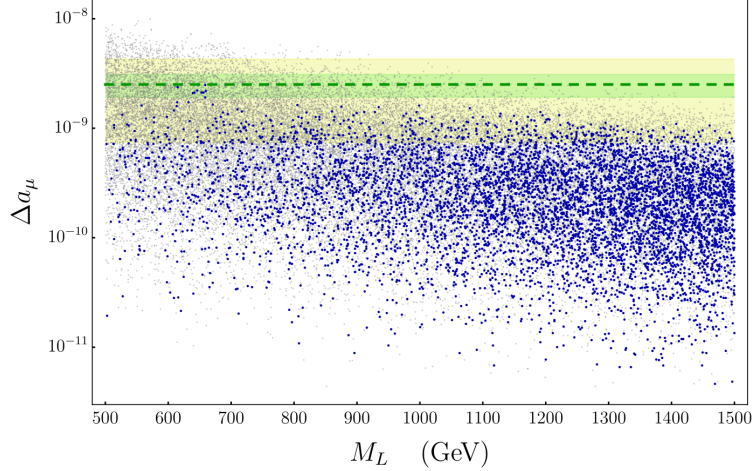


Figure 7: Δa_μ as a function of M_L . Dashed line, horizontal bands and color code as in Fig. 4.

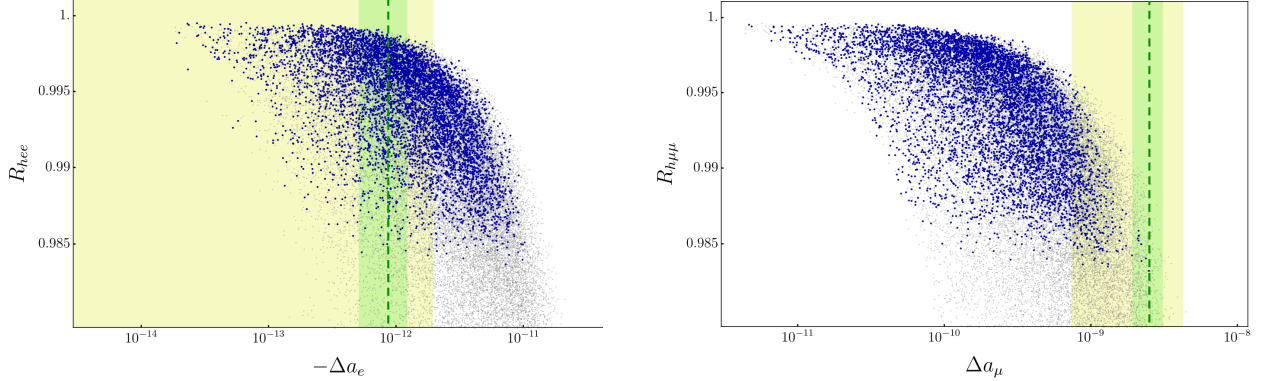


Figure 8: R_{hee} (left) and $R_{h\mu\mu}$ (right) as a function of Δa_e and Δa_μ , respectively. The vertical dashed lines represent the central values for Δa_e and Δa_μ , whereas 1σ (3σ) regions are displayed as yellow (green) bands.

where $\Gamma_{\text{SM}}(h \rightarrow \ell^+\ell^-)$ is the SM decay width, as a function of Δa_ℓ . In both cases, the reductions are small, at most of about $\sim 2\%$ in the parameter points that pass all the experimental bounds. This is due the fact that the $R_{h\ell\ell}$ ratios correlate with the corresponding $R_{Z\ell\ell}$ ratios, and are thus strongly constrained. Therefore, our setup predicts SM-like Higgs boson decays into charged leptons.

Finally, we have focused on a scenario with diagonal Y_Σ couplings in order to enhance the diagonal contributions to the muon $g-2$. This strongly suppresses all lepton flavor violating signals, which can only take place via the off-diagonal entries of the small μ parameter. We believe this to be a generic prediction of our model when the muon $g-2$ anomaly is addressed. However, we cannot discard the possibility of very fine-tuned parameter regions with large off-diagonal Y_Σ couplings and accidentally suppressed flavor violating transitions.

5 Discussion

The recent announcement of the first results by the Muon $g - 2$ collaboration at Fermilab has sparked a renewed interest in a long-standing anomaly. Together with the analogous discrepancy in the anomalous magnetic moment of the electron, they constitute a pair of intriguing deviations with respect to the SM predictions. If confirmed, new BSM states with masses not much above the electroweak scale will be required in order to address the discrepancies.

We have analyzed the electron and muon $g - 2$ in an extended version of the ISS3 model that includes a pair of VL doublet leptons. This model is motivated by the need to generate neutrino masses, which in this setup are induced at the electroweak scale. This naturally leads to a rich phenomenology in multiple fronts. Our analysis has taken into account the most relevant experimental bounds in our scenario. This includes limits from direct searches at the LHC, deviations in $Z \rightarrow \ell^+\ell^-$ decays and a compilation of electroweak limits. These are the main conclusions of our work:

- The pure ISS3 cannot address the electron and muon $g - 2$ anomalies due to the combination of the constraints on the m_D/M_Σ ratio derived from a variety of electroweak data and a strong chiral suppression of the order of m_ℓ/v .
- The inclusion of a VL lepton doublet pair to the ISS3 particle content suffices to enhance the contributions to the muon $g - 2$ and fully explain the observed discrepancy.
- The electron $g - 2$ anomaly can also be explained, in this case in a wider region of the parameter space.
- No significant change in the $h \rightarrow \ell^+\ell^-$ decays is found, and then these stay SM-like.

In this work we have focused on a minimal extension of the ISS3, containing only one VL lepton doublet pair. In principle, one may introduce additional copies of $L_{L,R}$ or VL lepton singlets, see for instance [41]. These non-minimal variations may reduce the impact of some of the bounds or enlarge the parameter space compatible with the current experimental hints in the muon $g - 2$. Furthermore, lepton number is explicitly broken in our model. Alternatively, one may consider the spontaneous breaking of a global $U(1)_L$ lepton number symmetry, leading to the appearance of a massless Goldstone boson, the majoron. However, a pure massless pseudoscalar state gives negative (lepton flavor conserving) contributions to the electron and muon anomalous magnetic moments [82], hence being unable to solve the tension in the case of the muon $g - 2$.

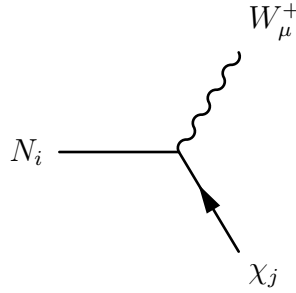
Exciting times are ahead of us. The muon $g - 2$ anomaly, now hinted by a second experiment, joins the list of results that have recently attracted attention to muons. It is natural to speculate about this anomaly together with the R_K and R_{K^*} anomalies found by the LHCb collaboration, as well as with the set of deviations observed in recent years in semileptonic $b \rightarrow s$ and $b \rightarrow c$ transitions. New experimental results, that may finally confirm an emerging picture beyond the SM, are eagerly awaited.

Acknowledgements

The authors are grateful to Martin Hirsch, Farinaldo Queiroz and Moritz Platscher for fruitful discussions and thank Ricardo Cepedello for help with the code. Work supported by the Spanish grants FPA2017-85216-P (MINECO/AEI/FEDER, UE), SEJI/2018/033 (Generalitat Valenciana) and FPA2017-90566-REDC (Red Consolider MultiDark). The work of PE is supported by the FPI grant PRE2018-084599. AV acknowledges financial support from MINECO through the Ramón y Cajal contract RYC2018-025795-I. The work of JTC is supported by the Ministerio de Ciencia e Innovación under FPI contract PRE2019-089992 of the SEV-2015-0548 grant and the grant PGC2018-102016-A-I00.

A Couplings

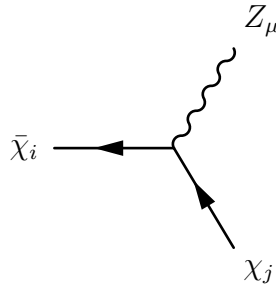
The couplings involved in the calculation of the charged lepton anomalous magnetic moments are shown in the Feynman diagrams of Fig. 1 and have been computed with the help of SARAH [83–87].⁸ We define them and list their analytical expressions here:



$$\mathcal{L}_{\chi NW} = \bar{N}_i \gamma^\mu \left[(g_{\chi NW}^L)_{ij} P_L + (g_{\chi NW}^R)_{ij} P_R \right] \chi_j W_\mu + \text{h.c.} \quad (47)$$

$$(g_{\chi NW}^L)_{ij} = -i g \left(\frac{1}{\sqrt{2}} \sum_{a=1}^3 \nu_{ja}^L \mathcal{U}_{ia} + \sum_{a=4}^9 \nu_{ja}^L \mathcal{U}_{ia} + \frac{1}{\sqrt{2}} \nu_{j10}^L \mathcal{U}_{i10} \right) \quad (48)$$

$$(g_{\chi NW}^R)_{ij} = -i g \left(\sum_{a=4}^9 \nu_{ja}^R \mathcal{U}_{ia}^* - \frac{1}{\sqrt{2}} \nu_{j10}^R \mathcal{U}_{i11}^* \right) \quad (49)$$

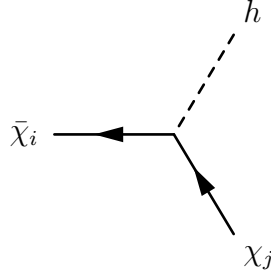


⁸See [88] for a pedagogical introduction to the use of SARAH.

$$\mathcal{L}_{\chi Z} = \bar{\chi}_i \gamma^\mu \left[(g_{\chi Z}^L)_{ij} P_L + (g_{\chi Z}^R)_{ij} P_R \right] \chi_j Z_\mu + \text{h.c.} \quad (50)$$

$$(g_{\chi Z}^L)_{ij} = \frac{i}{2} (g \cos \theta_W - g' \sin \theta_W) \left(\sum_{a=1}^3 \nu_{ja}^{L*} \nu_{ia}^L + \nu_{j10}^{L*} \nu_{i10}^L \right) + i g \cos \theta_W \sum_{a=4}^9 \nu_{ja}^{L*} \nu_{ia}^L \quad (51)$$

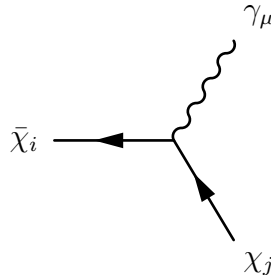
$$(g_{\chi Z}^R)_{ij} = -i g' \sin \theta_W \sum_{a=1}^3 \nu_{ia}^{R*} \nu_{ja}^R + i g \cos \theta_W \sum_{a=4}^9 \nu_{ia}^{R*} \nu_{ja}^R + \frac{i}{2} (g \cos \theta_W - g' \sin \theta_W) \nu_{i10}^{R*} \nu_{j10}^R \quad (52)$$



$$\mathcal{L}_{\chi h} = \bar{\chi}_i \left[(g_{\chi h}^L)_{ij} P_L + (g_{\chi h}^R)_{ij} P_R \right] \chi_j h + \text{h.c.} \quad (53)$$

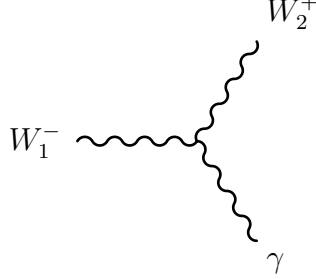
$$(g_{\chi h}^L)_{ij} = -\frac{i}{\sqrt{2}} \sum_{a,b=1}^3 \nu_{jb}^{L*} \nu_{ia}^{R*} (Y_e)_{ab} - i \sum_{a=1}^3 \sum_{b=1}^3 \nu_{jb}^{L*} \nu_{ia+3}^{R*} (Y_\Sigma)_{ab} \\ - i \nu_{j10}^{L*} \left[\sum_{a=1}^3 \nu_{ia+3}^{R*} (\lambda_L)_a + \frac{1}{\sqrt{2}} \sum_{a=1}^3 \nu_{ia}^{R*} (\lambda_R)_a \right] \quad (54)$$

$$(g_{\chi h}^R)_{ij} = -\frac{i}{\sqrt{2}} \sum_{a,b=1}^3 \nu_{ib}^L \nu_{ja}^R (Y_e)^*_{ab} - i \sum_{a=1}^3 \sum_{b=1}^3 \nu_{ib}^L \nu_{ja+3}^R (Y_\Sigma)^*_{ab} \\ - i \left[\sum_{a=1}^3 \nu_{ja+3}^R (\lambda_L^*)_a + \frac{1}{\sqrt{2}} \sum_{a=1}^3 \nu_{ja}^R (\lambda_R^*)_a \right] \nu_{i10}^L \quad (55)$$



$$\mathcal{L}_{\chi\gamma} = \bar{\chi}_i \gamma^\mu \left[(g_{\chi\gamma}^L)_{ij} P_L + (g_{\chi\gamma}^R)_{ij} P_R \right] \chi_j A_\mu + \text{h.c.} \quad (56)$$

$$(g_{\chi\gamma}^L)_{ij} = (g_{\chi\gamma}^R)_{ij} = i e \delta_{ij} \quad (57)$$



$$\mathcal{L}_{W\gamma} = \Gamma^{\mu\alpha\beta} W_\mu W_\alpha A_\beta \quad (58)$$

$$\Gamma^{\mu\alpha\beta} = -i g \sin \theta_W \left[g^{\alpha\beta} (p_{W_1}^\mu + p_{W_2}^\mu) + g^{\mu\beta} (-p_{W_2}^\alpha + p_\gamma^\alpha) + g^{\alpha\mu} (-p_\gamma^\beta - p_{W_1}^\beta) \right] \quad (59)$$

B Charged lepton anomalous magnetic moments: full expressions

We define the dimensionless quantities

$$\epsilon_{li} = \frac{m_\ell}{m_{\chi_i}}, \quad \delta_{li} = \frac{m_\ell}{m_{N_i}}, \quad \omega_{ai} = \frac{m_a}{m_{\chi_i}} \quad \text{and} \quad \omega_{Wi} = \frac{m_W}{m_{N_i}}, \quad (60)$$

with $a = Z, h$.

W contribution

The W contribution to the charged lepton anomalous magnetic moments can be written as

$$\Delta a_\ell(W) = \frac{1}{32\pi^2 \omega_{W_i}^2 \delta_{li}^4} \left[(C_{\chi NW}^2)_{i\ell} f_W(\delta_{li}^2, \omega_{W_i}^2) + \delta_{li} (D_{\chi NW}^2)_{i\ell} g_W(\delta_{li}^2, \omega_{W_i}^2) \right], \quad (61)$$

where a sum over the repeated index i is implicit and f_W and g_W are two loop functions given by

$$\begin{aligned}
f_W(x, y) &= x^3 + x^2(8y - 1) + 2x(1 + y - 2y^2) \\
&+ [3x^2y - x(1 - 3y + 5y^2) - 3y^2 + 2y^3 + 1] \log y \\
&+ \frac{2}{\Delta(x, y)} [3x^3y + x^2(1 - 8y^2) + x(7y^3 - 7y^2 + 2y - 2) \\
&+ (1 - y)^3(1 + 2y)] \log \frac{1 + y - x + \Delta(x, y)}{2\sqrt{y}}, \tag{62}
\end{aligned}$$

$$\begin{aligned}
g_W(x, y) &= 2x(1 + 2y) + [x(3y - 1) - 2y^2 + y + 1] \log y \\
&+ \frac{2}{\Delta(x, y)} [x^2(3y + 1) - x(2 - y + 5y^2) + 2y^3 - 3y^2 + 1] \log \frac{1 + y - x + \Delta(x, y)}{2\sqrt{y}}. \tag{63}
\end{aligned}$$

Here we have defined the auxiliary function

$$\Delta(x, y) = \sqrt{x^2 - 2x(1 + y) + (1 - y)^2}. \tag{64}$$

Z contribution

The Z contribution can be written as

$$\Delta a_\ell(Z) = \frac{1}{32\pi^2 \omega_{Zi}^2 \epsilon_{\ell i}^4} \left[(C_{\chi Z}^2)_{i\ell} f_Z(\epsilon_{\ell i}^2, \omega_{Zi}^2) + \epsilon_{\ell i} (D_{\chi Z}^2)_{i\ell} g_Z(\epsilon_{\ell i}^2, \omega_{Zi}^2) \right]. \tag{65}$$

Again, there is a sum over the repeated index i , whereas f_Z and g_Z are the loop functions

$$\begin{aligned}
f_Z(x, y) &= -x[x^2 + x(3 - 4y) + 4y^2 - 2y - 2] \\
&+ [x^2 - x(2 - 2y + 3y^2) + 2y^3 - 3y^2 + 1] \log y \\
&- \frac{2}{\Delta(x, y)} [x^3 + x^2(3y^2 + y - 3) - x(5y^3 - 4y^2 + 2y - 3) \\
&- (1 - y)^3(1 + 2y)] \log \frac{1 + y - x + \Delta(x, y)}{2\sqrt{y}}, \tag{66}
\end{aligned}$$

$$\begin{aligned}
g_Z(x, y) &= 2x(2x - 2y - 1) - [x^2 + x(y - 2) - 2y^2 + y + 1] \log y \\
&+ \frac{2}{\Delta(x, y)} [x^3 - 3x^2 + 3x(1 + y^2) - 2y^3 + 3y^2 - 1] \log \frac{1 + y - x + \Delta(x, y)}{2\sqrt{y}}. \tag{67}
\end{aligned}$$

h contribution

Finally, the h contribution to the charged leptons $g - 2$ can be written as

$$\Delta a_\ell(h) = \frac{1}{32\pi^2 \epsilon_{\ell i}^4} \left[(C_{\chi h}^2)_{i\ell} f_h(\epsilon_{\ell i}^2, \omega_{hi}^2) + \epsilon_{\ell i} (D_{\chi h}^2)_{i\ell} g_h(\epsilon_{\ell i}^2, \omega_{hi}^2) \right], \tag{68}$$

with an implicit sum over the repeated i index and the loop functions

$$f_h(x, y) = -x(x + 2y - 2) + [(1 - y)^2 - x] \log y + \frac{2}{\Delta(x, y)} [x^2 + x(y^2 + y - 2) + (1 - y)^3] \log \frac{1 + y - x + \Delta(x, y)}{2\sqrt{y}}, \quad (69)$$

$$g_h(x, y) = 2x - (x + y - 1) \log y + \frac{2}{\Delta(x, y)} [(1 - x)^2 + y^2 - 2y] \log \frac{1 + y - x + \Delta(x, y)}{2\sqrt{y}}. \quad (70)$$

We have compared our results to the general expressions provided in [65], finding full agreement. Our results also match those recently presented in [57], where a model with similar contributions to the muon $g - 2$ was considered. Finally, analytical expressions for the contributions to the muon $g - 2$ in the limit of heavy mediators are provided in [12]. While we do not consider this limit in our paper (since it would correspond to $m_W, m_Z, m_h \gg m_{N_i}, m_{\chi_i}$), it can be used to crosscheck our results. We find full agreement, with the only exception of the W contribution, where the expression given in [12] has the vector and axial couplings interchanged with respect to our result.

References

- [1] T. Aoyama, M. Hayakawa, T. Kinoshita, and M. Nio, “Tenth-Order QED Contribution to the Electron $g-2$ and an Improved Value of the Fine Structure Constant,” *Phys. Rev. Lett.* **109** (2012) 111807, [arXiv:1205.5368 \[hep-ph\]](#).
- [2] T. Aoyama, M. Hayakawa, T. Kinoshita, and M. Nio, “Complete Tenth-Order QED Contribution to the Muon $g-2$,” *Phys. Rev. Lett.* **109** (2012) 111808, [arXiv:1205.5370 \[hep-ph\]](#).
- [3] S. Laporta, “High-precision calculation of the 4-loop contribution to the electron $g-2$ in QED,” *Phys. Lett. B* **772** (2017) 232–238, [arXiv:1704.06996 \[hep-ph\]](#).
- [4] T. Aoyama, T. Kinoshita, and M. Nio, “Revised and Improved Value of the QED Tenth-Order Electron Anomalous Magnetic Moment,” *Phys. Rev. D* **97** no. 3, (2018) 036001, [arXiv:1712.06060 \[hep-ph\]](#).
- [5] **Muon $g-2$** Collaboration, G. Bennett *et al.*, “Final Report of the Muon E821 Anomalous Magnetic Moment Measurement at BNL,” *Phys. Rev. D* **73** (2006) 072003, [arXiv:hep-ex/0602035](#).
- [6] F. Jegerlehner and A. Nyffeler, “The Muon $g-2$,” *Phys. Rept.* **477** (2009) 1–110, [arXiv:0902.3360 \[hep-ph\]](#).
- [7] **RBC, UKQCD** Collaboration, T. Blum, P. Boyle, V. Gülpers, T. Izubuchi, L. Jin, C. Jung, A. Jüttner, C. Lehner, A. Portelli, and J. Tsang, “Calculation of the hadronic vacuum polarization contribution to the muon anomalous magnetic moment,” *Phys. Rev. Lett.* **121** no. 2, (2018) 022003, [arXiv:1801.07224 \[hep-lat\]](#).

- [8] **Muon $g - 2$** Collaboration, B. Abi *et al.*, “Measurement of the positive muon anomalous magnetic moment to 0.46 ppm,” *Phys. Rev. Lett.* **126** (2021) 141801.
- [9] T. Aoyama *et al.*, “The anomalous magnetic moment of the muon in the Standard Model,” *Phys. Rept.* **887** (2020) 1–166, [arXiv:2006.04822 \[hep-ph\]](#).
- [10] L. Morel, Z. Yao, P. Cladé, and S. Guellati-Khélifa, “Determination of the fine-structure constant with an accuracy of 81 parts per trillion,” *Nature* **588** no. 7836, (2020) 61–65.
- [11] A. Gérardin, “The anomalous magnetic moment of the muon: status of Lattice QCD calculations,” in *38th International Symposium on Lattice Field Theory*. 12, 2020. [arXiv:2012.03931 \[hep-lat\]](#).
- [12] M. Lindner, M. Platscher, and F. S. Queiroz, “A Call for New Physics : The Muon Anomalous Magnetic Moment and Lepton Flavor Violation,” *Phys. Rept.* **731** (2018) 1–82, [arXiv:1610.06587 \[hep-ph\]](#).
- [13] S. Borsanyi *et al.*, “Leading hadronic contribution to the muon 2 magnetic moment from lattice QCD,” [arXiv:2002.12347 \[hep-lat\]](#).
- [14] A. Crivellin, M. Hoferichter, C. A. Manzari, and M. Montull, “Hadronic Vacuum Polarization: $(g - 2)_\mu$ versus Global Electroweak Fits,” *Phys. Rev. Lett.* **125** no. 9, (2020) 091801, [arXiv:2003.04886 \[hep-ph\]](#).
- [15] G. F. Giudice, P. Paradisi, and M. Passera, “Testing new physics with the electron $g-2$,” *JHEP* **11** (2012) 113, [arXiv:1208.6583 \[hep-ph\]](#).
- [16] R. N. Mohapatra and J. W. F. Valle, “Neutrino Mass and Baryon Number Nonconservation in Superstring Models,” *Phys. Rev.* **D34** (1986) 1642. [[235\(1986\)](#)].
- [17] A. Abada, C. Biggio, F. Bonnet, M. B. Gavela, and T. Hambye, “Low energy effects of neutrino masses,” *JHEP* **12** (2007) 061, [arXiv:0707.4058 \[hep-ph\]](#).
- [18] M. B. Gavela, T. Hambye, D. Hernandez, and P. Hernandez, “Minimal Flavour Seesaw Models,” *JHEP* **09** (2009) 038, [arXiv:0906.1461 \[hep-ph\]](#).
- [19] D. Ibanez, S. Morisi, and J. W. F. Valle, “Inverse tri-bimaximal type-III seesaw and lepton flavor violation,” *Phys. Rev.* **D80** (2009) 053015, [arXiv:0907.3109 \[hep-ph\]](#).
- [20] E. Ma, “Inverse Seesaw Neutrino Mass from Lepton Triplets in the $U(1)_\Sigma$ Model,” *Mod. Phys. Lett.* **A24** (2009) 2491–2495, [arXiv:0905.2972 \[hep-ph\]](#).
- [21] O. J. P. Eboli, J. Gonzalez-Fraile, and M. C. Gonzalez-Garcia, “Neutrino Masses at LHC: Minimal Lepton Flavour Violation in Type-III See-saw,” *JHEP* **12** (2011) 009, [arXiv:1108.0661 \[hep-ph\]](#).
- [22] S. Morisi, E. Peinado, and A. Vicente, “Flavor origin of R-parity,” *J. Phys.* **G40** (2013) 085004, [arXiv:1212.4145 \[hep-ph\]](#).

- [23] J. A. Aguilar-Saavedra, P. M. Boavida, and F. R. Joaquim, “Flavored searches for type-III seesaw mechanism at the LHC,” *Phys. Rev.* **D88** (2013) 113008, [arXiv:1308.3226 \[hep-ph\]](#).
- [24] S. S. C. Law and K. L. McDonald, “Generalized inverse seesaw mechanisms,” *Phys. Rev.* **D87** no. 11, (2013) 113003, [arXiv:1303.4887 \[hep-ph\]](#).
- [25] S. Centelles Chuliá, R. Srivastava, and A. Vicente, “The Inverse Seesaw Family: Dirac And Majorana,” [arXiv:2011.06609 \[hep-ph\]](#).
- [26] A. Abada, C. Biggio, F. Bonnet, M. B. Gavela, and T. Hambye, “ $\mu \rightarrow e\gamma$ and $\tau \rightarrow l\gamma$ decays in the fermion triplet seesaw model,” *Phys. Rev.* **D78** (2008) 033007, [arXiv:0803.0481 \[hep-ph\]](#).
- [27] R. Franceschini, T. Hambye, and A. Strumia, “Type-III see-saw at LHC,” *Phys. Rev.* **D78** (2008) 033002, [arXiv:0805.1613 \[hep-ph\]](#).
- [28] A. Das and S. Mandal, “Bounds on the triplet fermions in type-III seesaw and implications for collider searches,” *Nucl. Phys. B* **966** (2021) 115374, [arXiv:2006.04123 \[hep-ph\]](#).
- [29] S. Mandal, J. C. Romão, R. Srivastava, and J. W. F. Valle, “Dynamical inverse seesaw mechanism as a simple benchmark for electroweak breaking and Higgs boson studies,” [arXiv:2103.02670 \[hep-ph\]](#).
- [30] A. Abada, M. E. Krauss, W. Porod, F. Staub, A. Vicente, and C. Weiland, “Lepton flavor violation in low-scale seesaw models: SUSY and non-SUSY contributions,” *JHEP* **11** (2014) 048, [arXiv:1408.0138 \[hep-ph\]](#).
- [31] C. Biggio, E. Fernandez-Martinez, M. Filaci, J. Hernandez-Garcia, and J. Lopez-Pavon, “Global Bounds on the Type-III Seesaw,” *JHEP* **05** (2020) 022, [arXiv:1911.11790 \[hep-ph\]](#).
- [32] W. Abdallah, A. Awad, S. Khalil, and H. Okada, “Muon Anomalous Magnetic Moment and $\mu \rightarrow e\gamma$ in $B - L$ Model with Inverse Seesaw,” *Eur. Phys. J. C* **72** (2012) 2108, [arXiv:1105.1047 \[hep-ph\]](#).
- [33] S. Khalil and C. S. Un, “Muon Anomalous Magnetic Moment in SUSY B-L Model with Inverse Seesaw,” *Phys. Lett. B* **763** (2016) 164–168, [arXiv:1509.05391 \[hep-ph\]](#).
- [34] J. Cao, J. Lian, L. Meng, Y. Yue, and P. Zhu, “Anomalous muon magnetic moment in the inverse seesaw extended next-to-minimal supersymmetric standard model,” *Phys. Rev. D* **101** no. 9, (2020) 095009, [arXiv:1912.10225 \[hep-ph\]](#).
- [35] L. T. Hue, P. N. Thanh, and T. D. Tham, “Anomalous Magnetic Dipole Moment $(g - 2)\mu$ in 3-3-1 Model with Inverse Seesaw Neutrinos,” *Commun. in Phys.* **30** no. 3, (2020) 221–230.

- [36] J. Cao, Y. He, J. Lian, D. Zhang, and P. Zhu, “Electron and Muon Anomalous Magnetic Moments in the Inverse Seesaw Extended NMSSM,” [arXiv:2102.11355 \[hep-ph\]](#).
- [37] T. Nomura, H. Okada, and P. Sanyal, “A radiatively induced inverse seesaw model with hidden $U(1)$ gauge symmetry,” [arXiv:2103.09494 \[hep-ph\]](#).
- [38] T. Mondal and H. Okada, “Inverse seesaw and $(g - 2)$ anomalies in $B - L$ extended two Higgs doublet model,” [arXiv:2103.13149 \[hep-ph\]](#).
- [39] L. T. Hue, H. T. Hung, N. T. Tham, t. H. N. Long, and T. Phong Nguyen, “Large $(g - 2)_\mu$ and signals of decays $e_b \rightarrow e_a \gamma$ in a 3-3-1 model with inverse seesaw neutrinos,” [arXiv:2104.01840 \[hep-ph\]](#).
- [40] A. E. Cárcamo Hernández, C. Espinoza, J. Carlos Gómez-Izquierdo, and M. Mondragón, “Fermion masses and mixings, dark matter, leptogenesis and $g - 2$ muon anomaly in an extended 2HDM with inverse seesaw,” [arXiv:2104.02730 \[hep-ph\]](#).
- [41] R. Dermisek and A. Raval, “Explanation of the Muon $g-2$ Anomaly with Vectorlike Leptons and its Implications for Higgs Decays,” *Phys. Rev. D* **88** (2013) 013017, [arXiv:1305.3522 \[hep-ph\]](#).
- [42] Z. Poh and S. Raby, “Vectorlike leptons: Muon $g-2$ anomaly, lepton flavor violation, Higgs boson decays, and lepton nonuniversality,” *Phys. Rev. D* **96** no. 1, (2017) 015032, [arXiv:1705.07007 \[hep-ph\]](#).
- [43] K. Kowalska and E. M. Sessolo, “Expectations for the muon $g-2$ in simplified models with dark matter,” *JHEP* **09** (2017) 112, [arXiv:1707.00753 \[hep-ph\]](#).
- [44] E. Megias, M. Quiros, and L. Salas, “ $g_\mu - 2$ from Vector-Like Leptons in Warped Space,” *JHEP* **05** (2017) 016, [arXiv:1701.05072 \[hep-ph\]](#).
- [45] C.-W. Chiang, H. Okada, and E. Senaha, “Dark matter, muon $g - 2$, electric dipole moments, and $Z \rightarrow \ell_i^+ \ell_j^-$ in a one-loop induced neutrino model,” *Phys. Rev. D* **96** no. 1, (2017) 015002, [arXiv:1703.09153 \[hep-ph\]](#).
- [46] L. Calibbi, R. Ziegler, and J. Zupan, “Minimal models for dark matter and the muon $g-2$ anomaly,” *JHEP* **07** (2018) 046, [arXiv:1804.00009 \[hep-ph\]](#).
- [47] J. Kawamura, S. Raby, and A. Trautner, “Complete vectorlike fourth family and new $U(1)$ ’ for muon anomalies,” *Phys. Rev. D* **100** no. 5, (2019) 055030, [arXiv:1906.11297 \[hep-ph\]](#).
- [48] L. Calibbi, M. L. López-Ibañez, A. Melis, and O. Vives, “Muon and electron $g - 2$ and lepton masses in flavor models,” *JHEP* **06** (2020) 087, [arXiv:2003.06633 \[hep-ph\]](#).
- [49] M. Frank and I. Saha, “Muon anomalous magnetic moment in two-Higgs-doublet models with vectorlike leptons,” *Phys. Rev. D* **102** no. 11, (2020) 115034, [arXiv:2008.11909 \[hep-ph\]](#).

- [50] E. J. Chun and T. Mondal, “Explaining $g - 2$ anomalies in two Higgs doublet model with vector-like leptons,” *JHEP* **11** (2020) 077, [arXiv:2009.08314 \[hep-ph\]](#).
- [51] N. Chakrabarty, “Doubly charged scalars and vector-like leptons confronting the muon $g-2$ anomaly and Higgs vacuum stability,” [arXiv:2010.05215 \[hep-ph\]](#).
- [52] K.-F. Chen, C.-W. Chiang, and K. Yagyu, “An explanation for the muon and electron $g - 2$ anomalies and dark matter,” *JHEP* **09** (2020) 119, [arXiv:2006.07929 \[hep-ph\]](#).
- [53] S. Jana, P. K. Vishnu, W. Rodejohann, and S. Saad, “Dark matter assisted lepton anomalous magnetic moments and neutrino masses,” *Phys. Rev. D* **102** no. 7, (2020) 075003, [arXiv:2008.02377 \[hep-ph\]](#).
- [54] R. Dermisek, K. Hermanek, and N. McGinnis, “Highly enhanced contributions of heavy Higgs bosons and new leptons to muon $g - 2$ and other observables,” [arXiv:2011.11812 \[hep-ph\]](#).
- [55] P. Das, M. K. Das, and N. Khan, “A new feasible dark matter region in the singlet scalar scotogenic model,” *Nucl. Phys. B* **964** (2021) 115307, [arXiv:2001.04070 \[hep-ph\]](#).
- [56] M. J. Baker, P. Cox, and R. R. Volkas, “Radiative Muon Mass Models and $(g - 2)_\mu$,” [arXiv:2103.13401 \[hep-ph\]](#).
- [57] R. Dermisek, K. Hermanek, and N. McGinnis, “Muon $g - 2$ in two Higgs doublet models with vectorlike leptons,” [arXiv:2103.05645 \[hep-ph\]](#).
- [58] P. Das, M. Kumar Das, and N. Khan, “The FIMP-WIMP dark matter and Muon $g-2$ in the extended singlet scalar model,” [arXiv:2104.03271 \[hep-ph\]](#).
- [59] C.-W. Chiang and K. Yagyu, “Radiative Seesaw Mechanism for Charged Leptons,” [arXiv:2104.00890 \[hep-ph\]](#).
- [60] C. Arbeláez, R. Cepedello, R. M. Fonseca, and M. Hirsch, “ $(g - 2)$ anomalies and neutrino mass,” *Phys. Rev. D* **102** no. 7, (2020) 075005, [arXiv:2007.11007 \[hep-ph\]](#).
- [61] D. Buttazzo and P. Paradisi, “Probing the muon $g-2$ anomaly at a Muon Collider,” [arXiv:2012.02769 \[hep-ph\]](#).
- [62] W. Yin and M. Yamaguchi, “Muon $g - 2$ at multi-TeV muon collider,” [arXiv:2012.03928 \[hep-ph\]](#).
- [63] R. Capdevilla, D. Curtin, Y. Kahn, and G. Krnjaic, “A No-Lose Theorem for Discovering the New Physics of $(g - 2)_\mu$ at Muon Colliders,” [arXiv:2101.10334 \[hep-ph\]](#).
- [64] G. 't Hooft, “Naturalness, chiral symmetry, and spontaneous chiral symmetry breaking,” *NATO Sci. Ser. B* **59** (1980) 135–157.

- [65] A. Crivellin, M. Hoferichter, and P. Schmidt-Wellenburg, “Combined explanations of $(g - 2)_{\mu,e}$ and implications for a large muon EDM,” *Phys. Rev. D* **98** no. 11, (2018) 113002, [arXiv:1807.11484 \[hep-ph\]](#).
- [66] H. H. Patel, “Package-X: A Mathematica package for the analytic calculation of one-loop integrals,” *Comput. Phys. Commun.* **197** (2015) 276–290, [arXiv:1503.01469 \[hep-ph\]](#).
- [67] S. M. Barr and A. Zee, “Electric Dipole Moment of the Electron and of the Neutron,” *Phys. Rev. Lett.* **65** (1990) 21–24. [Erratum: *Phys.Rev.Lett.* 65, 2920 (1990)].
- [68] P. F. de Salas, D. V. Forero, S. Gariazzo, P. Martínez-Miravé, O. Mena, C. A. Ternes, M. Tórtola, and J. W. F. Valle, “2020 global reassessment of the neutrino oscillation picture,” *JHEP* **02** (2021) 071, [arXiv:2006.11237 \[hep-ph\]](#).
- [69] I. Cordero-Carrión, M. Hirsch, and A. Vicente, “Master Majorana neutrino mass parametrization,” *Phys. Rev. D* **99** no. 7, (2019) 075019, [arXiv:1812.03896 \[hep-ph\]](#).
- [70] I. Cordero-Carrión, M. Hirsch, and A. Vicente, “General parametrization of Majorana neutrino mass models,” *Phys. Rev. D* **101** no. 7, (2020) 075032, [arXiv:1912.08858 \[hep-ph\]](#).
- [71] J. A. Casas and A. Ibarra, “Oscillating neutrinos and $\mu \rightarrow e, \gamma$,” *Nucl. Phys. B* **618** (2001) 171–204, [arXiv:hep-ph/0103065](#).
- [72] A. Crivellin and M. Hoferichter, “Consequences of chirally enhanced explanations of $(g - 2)_{\mu}$ for $h \rightarrow \mu\mu$ and $Z \rightarrow \mu\mu$,” [arXiv:2104.03202 \[hep-ph\]](#).
- [73] **Particle Data Group** Collaboration, P. A. Zyla *et al.*, “Review of Particle Physics,” *PTEP* **2020** no. 8, (2020) 083C01.
- [74] **CMS** Collaboration, A. M. Sirunyan *et al.*, “Evidence for Higgs boson decay to a pair of muons,” *JHEP* **01** (2021) 148, [arXiv:2009.04363 \[hep-ex\]](#).
- [75] S. Fajfer, J. F. Kamenik, and M. Tamaro, “Interplay of New Physics Effects in $(g - 2)_{\ell}$ and $h \rightarrow \ell^+ \ell^-$ – Lessons from SMEFT,” [arXiv:2103.10859 \[hep-ph\]](#).
- [76] **ATLAS** Collaboration, G. Aad *et al.*, “Search for type-III seesaw heavy leptons in dilepton final states in pp collisions at $\sqrt{s} = 13$ TeV with the ATLAS detector,” *Eur. Phys. J. C* **81** no. 3, (2021) 218, [arXiv:2008.07949 \[hep-ex\]](#).
- [77] **CMS** Collaboration, S. Chatrchyan *et al.*, “Search for Heavy Lepton Partners of Neutrinos in Proton-Proton Collisions in the Context of the Type III Seesaw Mechanism,” *Phys. Lett. B* **718** (2012) 348–368, [arXiv:1210.1797 \[hep-ex\]](#).
- [78] **CMS** Collaboration, A. M. Sirunyan *et al.*, “Search for Evidence of the Type-III Seesaw Mechanism in Multilepton Final States in Proton-Proton Collisions at $\sqrt{s} = 13$ TeV,” *Phys. Rev. Lett.* **119** no. 22, (2017) 221802, [arXiv:1708.07962 \[hep-ex\]](#).

- [79] C. Biggio and F. Bonnet, “Implementation of the Type III Seesaw Model in FeynRules/MadGraph and Prospects for Discovery with Early LHC Data,” *Eur. Phys. J. C* **72** (2012) 1899, [arXiv:1107.3463 \[hep-ph\]](#).
- [80] A. Falkowski, D. M. Straub, and A. Vicente, “Vector-like leptons: Higgs decays and collider phenomenology,” *JHEP* **05** (2014) 092, [arXiv:1312.5329 \[hep-ph\]](#).
- [81] F. F. Freitas, J. a. Gonçalves, A. P. Morais, and R. Pasechnik, “Phenomenology of vector-like leptons with Deep Learning at the Large Hadron Collider,” *JHEP* **01** (2021) 076, [arXiv:2010.01307 \[hep-ph\]](#).
- [82] P. Escribano and A. Vicente, “Ultralight scalars in leptonic observables,” *JHEP* **03** (2021) 240, [arXiv:2008.01099 \[hep-ph\]](#).
- [83] F. Staub, “SARAH,” [arXiv:0806.0538 \[hep-ph\]](#).
- [84] F. Staub, “From Superpotential to Model Files for FeynArts and CalcHep/CompHep,” *Comput. Phys. Commun.* **181** (2010) 1077–1086, [arXiv:0909.2863 \[hep-ph\]](#).
- [85] F. Staub, “Automatic Calculation of supersymmetric Renormalization Group Equations and Self Energies,” *Comput. Phys. Commun.* **182** (2011) 808–833, [arXiv:1002.0840 \[hep-ph\]](#).
- [86] F. Staub, “SARAH 3.2: Dirac Gauginos, UFO output, and more,” *Comput. Phys. Commun.* **184** (2013) 1792–1809, [arXiv:1207.0906 \[hep-ph\]](#).
- [87] F. Staub, “SARAH 4 : A tool for (not only SUSY) model builders,” *Comput. Phys. Commun.* **185** (2014) 1773–1790, [arXiv:1309.7223 \[hep-ph\]](#).
- [88] A. Vicente, “Computer tools in particle physics,” [arXiv:1507.06349 \[hep-ph\]](#).